Desalination and Water Treatment
www.deswater.com

doi: 10.5004/dwt.2018.22000

117 (2018) 21–31
June

Properties and the application of polyacrylonitrile membranes with the addition of nanotubes for heavy metals removal

Lucyna Przywara[a,*], Beata Fryczkowska[b], Dorota Biniaś[b], Czesław Ślusarczyk[b], Janusz Fabia[b], Jarosław Janicki[b]

[a]*Faculty of Materials, Civil and Environmental Engineering, Institute of Environmental Protection and Engineering, University of Bielsko-Biała, Willowa 2, 43-309 Bielsko-Biała, Poland, Tel. +48 338279114; Fax: +48 33 8279101; email: l.przywara@ath.bielsko.pl*
[b]*Faculty of Materials, Civil and Environmental Engineering, Institute of Textile Engineering and Polymer Materials, University of Bielsko-Biała, Willowa 2, 43-309 Bielsko-Biała, Poland, emails: bfryczkowska@ath.bielsko.pl (B. Fryczkowska), dbinias@ath.bielsko.pl (D. Biniaś), cslusarczyk@ath.bielsko.pl (C. Ślusarczyk), jfabia@ath.bielsko.pl (J. Fabia), jjanicki@ath.bielsko.pl (J. Janicki)*

Received 7 December 2017; Accepted 4 February 2018

ABSTRACT

The paper presents results of research on the production, properties and application of polyacrylonitrile (PAN) based membranes with the addition of multiwallet carbon nanotubes (MWCNT) for the removal of heavy metals such as lead, zinc, cobalt and nickel. The research has shown that the introduction of nanotubes into a PAN matrix results in increased mass per unit area, thickness, water sorption, porosity, pore size of the membranes and hydrophobic properties of their surfaces. Moreover, the modifier improved the transport and separation properties of MWCNT/PAN composite membranes. The use of 0.1% MWCNT addition in the PAN matrix increased the distilled water flux through the membrane 9, 11 and 12 times at transmembrane pressure amounting to 0.1, 0.15 and 0.2 MPa, respectively. The degree of heavy metals removal for all the obtained membranes was determined by atomic absorption spectrometry and for subsequent ions was: 100% (Co^{2+}), 72 ÷ 100% (Zn^{2+}), 70 ÷100% (Ni^{2+}) and 65 ÷ 100% (Pb^{2+}). The instrumental methods used, including: scanning electron microscopy, Fourier transform infrared spectroscopy, wide-angle X-ray scattering, differential scanning calorimetry and thermogravimetric analysis, demonstrated the impact of MWCNT addition on structural composition of produced composite membranes and confirmed the high degree of the modifier dispersion in the polymer matrix.

Keywords: Polyacrylonitrile; Carbon nanotubes; Heavy metals; Membrane; Transport properties; Rejection

1. Introduction

Micropollution of the environment has been the subject of research since the early 1980s. It was then that polycyclic aromatic hydrocarbons, surfactants, chlorinated organic compounds, as well as heavy metals and radioactive particles were isolated. In the water environment, micropollution occurs because commonly used wastewater treatment technologies are unable to remove the substances present completely.

Heavy metals enter the environment mainly with industrial effluents, which are not pretreated or treated, being introduced into waters or municipal sewage. These compounds are primarily found in industrial effluents and may come from galvanizing plants, mining processes, battery manufacturing processes, paint and pigment production, as well as from glassworks. These wastewaters usually contain copper (Cu), chromium (Cr), cadmium (Cd), lead (Pb) and nickel (Ni) compounds, which are non-biodegradable and accumulate in aquatic organisms with which they enter the trophic chain, posing a threat to

* Corresponding author.

Presented at the 13th Conference on Microcontaminants in Human Environment, 4–6 December 2017, Czestochowa, Poland.

human health and even life [1]. Methods used to remove metals from industrial effluents are based on reactions of hydroxides or metal sulphides precipitation [2,3], adsorption on various materials [4], integrated system electrocoagulation–phytoremediation [5], ion exchange (on ion exchange chelators), concentration and membrane methods [6].

Polyacrylonitrile (PAN) is a well-known engineering polymer that is widely used in membrane techniques: ultrafiltration (UF), nanofiltration (NF), reverse osmosis and pervaporation (PV). Since the polymer is soluble in many solvents, the production of PAN membranes is based on the phase inversion wet method. Hydrophobic PAN membranes can be hydrophobized by physical or chemical modification. Another way to change the properties of this polymer is introducing various additions to obtain composite materials. Inorganic (metal oxides or metal nanoparticles) or carbon (fullerenes, nanotubes, graphene oxide and graphene) components can be used as PAN modifiers.

Carbon nanotubes (CNTs) are well-known and described supermolecular structures that have excellent mechanical, thermal and electrical properties that result from their length to diameter ratio, surface smoothness and hydrophobicity [7]. These properties allow the use of nanotubes in the production of unique composites that are widely used in water treatment techniques, as cheap adsorbents [8] and membranes for UF [9], NF [10], PV [5], membrane distillation [5] and gas separation membrane process [11]. Membranes with the addition of nanotubes are obtained using polyethersulphone [12], cellulose esters [13], polymethyl methacrylate [11], polyvinylidene fluoride [14], polyimide [15], polypyrrole [10] and polypropylene [16].

The literature also provides many examples of how nanotube-modified PAN composite membranes are obtained. You et al. [17] obtained composite membranes from PAN nanofibres, which were the carrier layer on which they applied a layer of polyvinyl alcohol nanofibres, with multiwallet carbon nanotubes (MWCNT) addition. Other researchers have used the electrospinning process to obtain filter membranes [18]. Xu et al. [19] produced nano-nonwovens by incorporating nanotubes onto the PAN/PP composite membrane using electrospraying. Palade et al. [20] obtained a PAN and non-functionalized MWCNT composite by evaporating the solvent [20]. Composite membranes from 14% PAN solution in *N*,*N*-dimethylformamide (DMF) were obtained by Majeed et al. [9] using 0.5%, 1% and 2% addition of functionalized CNTs and Dastbaz et al. [21] used the same concentrations of functionalized MWCNT, but the PAN concentration was slightly higher (15%).

Palade et al. [20] studies have shown that it is possible to obtain a well dispersed PAN composite with unmodified MWCNT. This paper presents the results of previously unreported studies on the use of unmodified CNTs for the preparation of MWCNT/PAN composite membranes. Unlike Palade et al. [20], method used for forming membranes is phase inversion by wet process. The work presents the influence of the additive MWCNT on the properties of PAN membranes and the possibility of their application for the removal of selected heavy metals from water and wastewater.

2. Experimental

2.1. Materials

PAN (MW = 85,000) copolymer (93.9% acrylonitrile/5.8% methyl acrylate/0.3% methallyl sulphonate) was purchased from Goodfellow Cambridge Ltd., England. NC7000™ nanotubes (MWCNT) were purchased from Nanocyl Sambreville, Belgium. $NaNO_3$, 98% H_2SO_4, $KMnO_4$, 30% H_2O_2, DMF, NaCl, $Co(NO_3)_2$, $Ni(NO_3)_2$, $Pb(NO_3)_2$ and $ZnCl_2$ were purchased from Avantor Performance Materials Poland S.A.

2.2. Membrane formation

PAN membranes were obtained using phase inversion method. First, a 12% solution of PAN in DMF was prepared. Membrane-forming solutions containing the appropriate amounts of components were prepared to form MWCNT/PAN composite membranes (Table 1). To this end, PAN and MWCNT were introduced into the solvent (DMF) and thoroughly mixed until a homogeneous solution was obtained.

The prepared solutions were then poured onto a clean glass plate and spread using a casting knife with an adjustable thickness fixed at 0.2 mm. Finally, the polymer film was rapidly coagulated in distilled water at room temperature until the membrane detached from the glass. The precipitated membranes were dried in air.

2.3. Membrane properties characterization

The thickness (l) of the membranes was measured with an Elmetron MG-1 thickness gauge. The contact angle (θ_c) of the skin layer of the membranes was measured using the FIBRO System AB PG-1 goniometer. The mass per unit area (W_s, g/cm^2) and the apparent density (d_m, g/cm^3) of the membranes were calculated using the following Eqs. (1) and (2):

$$W_s = \frac{w}{s} \tag{1}$$

$$d_m = \frac{w}{s \cdot l} \tag{2}$$

where w is the mass of a membrane with an area of 1 cm^2, s is the membrane surface area (cm^2) and l is the membrane thickness (cm).

To perform the water sorption (U) measurements, dry membrane samples were weighed (W_d), then placed in a distilled water beaker for 10 s and then squeezed in filter paper and reweighed in wet condition (W_w). The sorption of water was calculated according to Eq. (3):

$$U = \frac{W_w - W_d}{W_d} 100\% \tag{3}$$

Table 1
Composition of membrane-forming solutions

Membrane designation	"0"	A	B	C
Amount of MWCNT (% w/w)	0	0.1	0.5	1
Amount of PAN (% w/w)	12	12	12	12
Amount of DMF (% w/w)	88	87.9	87.5	83

The porosity of the membranes (ε), which is defined as the ratio of pore volume to the volume of the membrane, was calculated using the following Eq. (4):

$$\varepsilon = \frac{\left(W_w - W_d\right)/d_w}{\left(W_w - W_d\right)/d_w + W_d/d_p}100\% \quad (4)$$

where d_w is the density of distilled water (0.998 g/cm^3) and d_p is the polymer density (1.184 g/cm^3) [22].

2.4. Measurements of water flux

The transport properties of the formed membranes were tested using a Millipore Amicon 8400 UF cell with a 350 mL capacity and a 7.6 cm membrane diameter that was equipped with an equalizing tank with an 800 mL capacity. First, dry membranes were immersed in distilled water for 1 h. Then, they were treated with distilled water for an additional 2 h under a pressure of 0.2 MPa to improve the membrane stability. UF tests were performed at operational pressures of 0.1, 0.15 or 0.2 MPa. Permeate flux (J_v) was calculated using the following Eq. (5):

$$J_v = \frac{Q}{At} \quad (5)$$

where J_v is the water flux (L/m^2 h), Q is the permeate volume (L), A is the effective membrane area (m^2) and t is the permeation time (h).

Pore size (r_m) was calculated on the basis of the specific permeate flux and porosity using the Guerout–Elford–Ferry equation [23] (6):

$$r_m = \sqrt{\frac{\left(2.9 - 1.75\varepsilon\right)8\eta l Q}{\varepsilon A \Delta P}} \quad (6)$$

where η is the water viscosity (8.9 × 10^{-4} Pa s), l is the membrane thickness (m), Q is the volume of permeated pure water per unit time (m^3/s), ε is the porosity of membranes, A is the effective membrane area (m^2) and ΔP is the operational pressure.

2.5. Measurements of rejection

Standard solutions of salts: NaCl, $Pb(NO_3)_2$, $Co(NO_3)_2$, $Ni(NO_3)_2$ and $ZnCl_2$ at concentrations of 6 mg/L were prepared to test the separation properties of the membranes obtained in the experiment. In addition, industrial wastewater from one of the electroplating plants in Silesian Voivodeship was used in the investigation. Industrial effluents were pretreated using Magnafloc 336 flocculant as described in our previous works [24,25]. Then, the concentration of selected metals (Zn, Co, Ni, Pb) was determined by means of atomic absorption spectrometry (AAS) and summarized in Table 2.

Then, 200 mL of successive standard solutions of metals and electroplating wastewater were added to the UF cell with the test membrane and the stirrer (stirring of the feed solution allows to avoid fouling). The permeation process was carried out at an operational pressure of 0.2 MPa and 20 mL doses of permeate were tapped, measuring simultaneously the time of the permeate discharge from the test tank. Permeate flux (J_v) was calculated using Eq. (1), assuming that in this case Q is the permeate volume (specific test solution).

Table 2
Concentration of ions of selected metals in pretreated electroplating wastewater

Identified metal	Quantity (mg/L)
Zn	0.61
Co	0.05
Ni	0.03
Pb	2.07

Ion concentrations of the subsequent metals were determined using AAS (Perkins-Elmer Atomic Absorption Spectrometry Analist 100 spectrometer), and then rejection coefficient was calculated using Eq. (7):

$$R = \left(1 - \frac{C_p}{C_f}\right)100\% \quad (7)$$

where R is the rejection performance of the membrane (%) and C_p and C_f are the concentrations of metal ions in the permeate and feed solution (mg/L), respectively.

2.6. Analytical methods

All measurements were performed using a Nicolet 6700 FT-IR spectrometer (Thermo Electron Corp., Madison, WI, USA) equipped with a Photoacoustics MTEC model 300 accessory. Samples for photoacoustic testing were placed in a special holder. The following measurement parameters were used: resolution, 4 cm^{-1}; spectral range, 500–4,000 cm^{-1}; (DTGS) detector; number of scans, 64. Data collection and post-processing were performed using OMNIC software (v. 8.0, Thermo Electron Corp.).

X-ray diffraction (XRD) investigations were performed with a URD 63 Seifert diffractometer. Cu Ka radiation was used at 40 kV and 30 mA. Monochromatization of the beam was obtained by means of a nickel filter and a pulse-height analyzer. A scintillation counter was used as a detector. Diffractograms were recorded from 18° to 26° with a step of 0.01°. Each diffraction curve was corrected for polarization, the Lorentz factor and incoherent scattering.

Thermal studies were realized using the TA Instruments equipment. Calorimetric investigations were done with MDSC 2920 differential scanning calorimeter. Measurements were performed under a nitrogen atmosphere (flow rate 40 mL/min) with the heating and cooling rate of 10°C/min and 60°C/min, in a temperature range from –10°C and –40°C to 320°C, respectively. Thermogravimetric analysis (TGA) investigations were performed using thermogravimetric analyzer Q500. Measurements were done while heating at 20°C/min from ambient to 800°C also in nitrogen atmosphere (flow 40 mL/min). The differential scanning calorimetry (DSC) and TGA curves obtained were analyzed using the TA Instruments Universal v4.5 and v4.7A software packages.

Membrane surface morphologies and their cross-sections were observed using a JSM 5500 LV JEOL scanning electron microscope. All samples were coated with a layer of gold in a JEOL JFC 1200 vacuum coater at 3×10^{-5} Torr.

3. Results and discussion

3.1. Membrane characteristics

As a result of the experiment PAN membranes ("0") and composite membranes (A–C) which differed in colour depending on the amount of MWCNT addition were obtained (Fig. 1). The skin layer of membrane "0" is white, while the other MWCNT/PAN composite membranes are grey. The membrane A (0.83% w/w MWCNT) is light grey while the membrane C (8.3% w/w MWCNT) is dark grey.

The paper presents the investigation of the physicochemical properties of the pure PAN membranes and MWCNT/PAN composite membranes obtained in the experiment (Table 3). These investigations covered mass per unit area, thickness, apparent density, contact angle, porosity and sorption properties.

The study of membrane thickness has shown that the thinnest membrane is membrane "0," while the other MWCNT/PAN composite membranes are approximately two times thicker. The obtained results allow to conclude that the membrane thickness is undoubtedly affected by the properties of the components of the membrane-forming solution and in particular by their polarity [26]. The results of the mass per unit area calculations showed that the pure PAN membrane is the lightest (~17.6 g/cm^2), which, combined with its thickness (~119 μm), results in an apparent density of ~0.148 g/cm^3. The apparent density of this membrane is eight times lower than the density of the pure polymer, indicating its porosity confirmed by the porosity calculations: ~58%.

The thickness of MWCNT/PAN composite membranes is in the range of 205.88 ÷ 223.53 μm, while their apparent density is 0.110 ÷ 0.162 g/cm^3. Membrane C is the thickest and has the highest apparent density. Compared with membrane "0," the composite membranes are characterized by a higher mass per unit area, which is increased as follows: 22.75 ± 0.92 (membrane A), 24.95 ± 0.85 (membrane B) and 36.10 ± 1.03 (membrane C). The obtained result may be a consequence of a hydrophobic addition whose mass fraction in the whole mass of the membranes is successively 0.83%, 4.2% and 8.3%. The porosity of the composite membranes is slightly decreasing as follows: 67.6% (membrane A), 66.2% (membrane B) and 64.5% (membrane C).

The contact angle studies confirmed the hydrophilic nature of the pure PAN membrane (~53°), while MWCNT-modified membranes have hydrophobic properties. The contact angle measured at the surface of the membrane skin layer is ~137° (membrane A), ~134° (membrane B) and ~ 131° (membrane C). Surprisingly, the results of sorption study show that the hydrophilic membrane "0" adsorbs only 117.9% ± 10.1% of water while the MWCNT/PAN composite membranes sorb more water. Low sorption for membrane "0" may result from low thickness, mass per unit area, porosity and high apparent density. Composite membranes are thicker, heavier and more porous, allowing for sorption in the order of ~176% (membrane A), ~165% (membrane B) and ~154% (membrane C).

3.2. Transport properties and pore sizes of membranes

Important parameters determining the transport properties of the membranes are the specific permeate flux and the pore size (Fig. 2).

It was observed during the investigation (Fig. 2(a)) that the unmodified membrane "0" has the lowest transport properties, which for the successive transmembrane

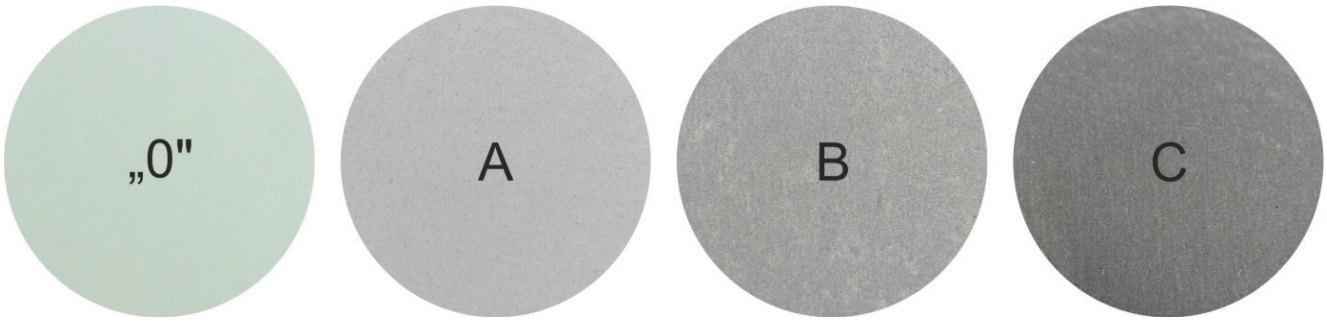

Fig. 1. Images of membrane "0" (pure PAN) and MWCNT/PAN composite membranes.

Table 3
Properties of the obtained membranes

Membrane	Thickness, l (μm)	Mass per unit area, W_s (g/m^2)	Apparent density, d_m (g/cm^3)	Contact angle, θ_c (°)	Sorption of water, U (%)	Porosity, ε (%)
"0"	118.9 ± 9.3	17.60 ± 0.56	0.148 ± 0.008	53.33 ± 1.5	117.9 ± 10.1	58.2 ± 3.2
A	207.3 ± 8.5	22.75 ± 0.92	0.110 ± 0.007	137.3 ± 2.1	176.3 ± 12.3	67.6 ± 3.0
B	205.9 ± 10.0	24.95 ± 0.85	0.121 ± 0.009	134.4 ± 5.8	165.4 ± 12.4	66.2 ± 2.9
C	223.5 ± 10.0	36.10 ± 1.03	0.162 ± 0.013	131.0 ± 3.5	154.0 ± 10.3	64.5 ± 5.1

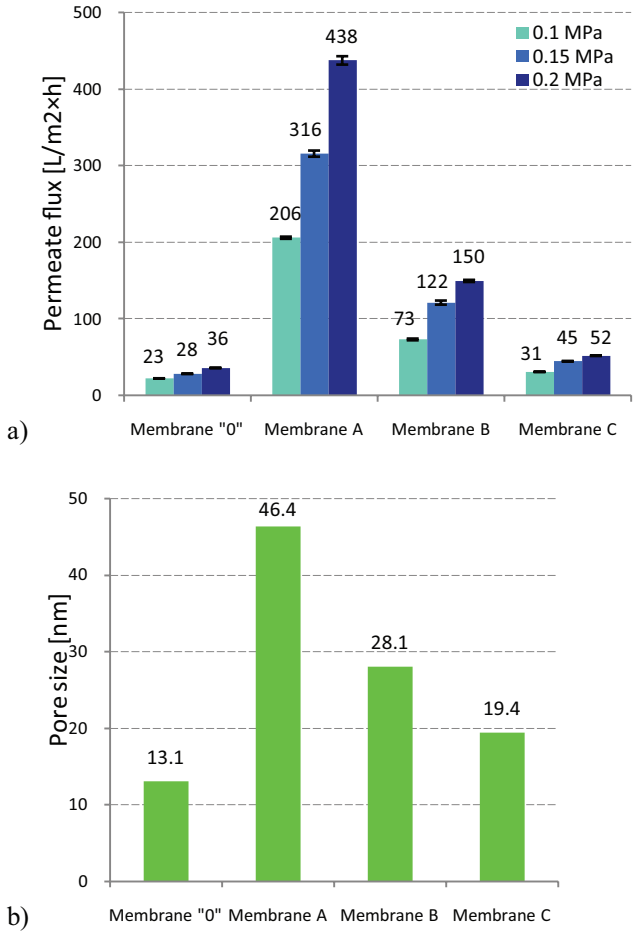

Fig. 2. Test results of (a) water flux and (b) pore sizes of pure PAN membranes and MWCNT/PAN composite membranes.

pressure (0.1, 0.15 and 0.2 MPa) are: 22.53 ± 0.16, 28.48 ± 0.27 and 36.23 ± 0.50 L/m² h, respectively. The results are confirmed by the SEM images (Fig. 6-1), which show that the membrane has a compact structure. On the other hand, the use of 0.1:12 (wt%) of MWCNT addition improves flux through the modified membranes 9–12 times. Membranes A are characterized by the following values of the volumetric permeate flux: 206.24 ± 1.41 (0.1 MPa), 316.05 ± 4.02 (0.15 MPa) and 437.80 ± 5.48 (0.2 MPa) L/m² h. Further addition of PAN results in a decrease in the transporting properties which, for membrane B, are 73.43 ± 1.14, 121.51 ± 2.69 and 149.84 ± 1.39 L/m² h for respective transmembrane pressure. For membrane C, the flux of distilled water for subsequent pressures is 31.07 ± 0.31, 44.91 ± 0.45 and 52.10 ± 0.30 L/m² h, respectively. Thus, the conducted studies have shown that MWCNT addition to PAN results in membranes with good transport properties, as confirmed by SEM microphotographs (Fig. 6-1). The results obtained for membrane A are higher than those obtained by Majeed et al. [9] and Dastbaz et al. [21].

For all studied membranes, the pore size was estimated (Fig. 2(b)) that impacts such variables as porosity, thickness or specific permeate flux. The pure PAN membrane has the smallest pores of all used membranes: 13.1 nm. The use of low MWCNT addition in the PAN matrix results in the formation of pores whose size was estimated at 46.4 nm (membrane A), which is 3.5 times more compared with membrane "0." Composite membranes B and C exhibit a pore size: 28.1 nm (membrane B) and 19.4 nm (membrane C), as clearly visible in SEM images (Fig. 6-1). The pore size calculations allowed to conclude that the addition of MWCNT introduced into the membrane evidently affects the morphology of the membrane structure. It is observed that as the density of MWCNT/PAN composite membranes increases, their porosity, water sorption, pore size and transport properties decrease. The obtained results may confirm that with the increase in the number of nanotubes, porous membranes are formed, but their pores are sealed (Fig. 6-1).

Studies on the transport properties of membranes based on pure PAN and MWCNT/PAN composites indicated the possibility of using the obtained membranes for the separation of heavy metals. Initially, each of the membranes was tested using aqueous solution containing Na(I), Zn(II), Ni(II), Co(II) and Pb(II) metal ions. The electroplating wastewater was then investigated for the same metal ions as for standard solutions (Table 3).

The study (Fig. 3) clearly demonstrated that the use of metal ions results in an increase in volumetric permeate flux. The increase in flux applies to all types of obtained membranes. For the membrane "0" the volumetric permeate flux increased 5–8 times and was: ~158 L/m² h (sodium ions), ~179 L/m² h (zinc ions), ~241 L/m² h (nickel ions), ~274 L/m² h (cobalt ions) and ~300 L/m² h (lead ions), respectively. In turn, the flow of electroplating wastewater through membrane "0" caused a three-fold increase in volumetric permeate flux, which was ~113 L/m² h. Composite membrane A was characterized by approximately two-fold increase in the permeate flux, which was: ~942 L/m² h (for Ni^{2+}), ~909 L/m² h (for Co^{2+}), ~870 L/m² h (for Pb^{2+}), ~865 L/m² h (for Zn^{2+}) and ~484 L/m² h (for Na^{+}), respectively. The study of the permeate flux for electroplating wastewater through membrane A, showed a slight increase in flux up to ~522 L/m² h. The study of the transport properties of membrane B showed that the flux of liquid increased 1–3 times from Zn^{2+} (~155 L/m² h), through Ni^{2+} (~264 L/m² h), Na^{+} (~269 L/m² h), Co^{2+} (~305 L/m² h) up to Pb^{2+} (~344 L/m² h). In turn, the flow of electroplating wastewater through membrane B caused a three-fold increase in volumetric permeate flux, which was ~484 L/m² h. The permeate flux for membrane C increased from 2.5 to 5 times and was: ~129 L/m² h (Zn ions), ~185 L/m² h (Ni ions), 192.09 ± 7.05 (Na ions), ~227 L/m² h (Pb ions), ~230 L/m² h (Co ions) and ~268 L/m² h (electroplating wastewater), respectively.

Analyzing the obtained results (Fig. 3), it can be seen that the membranes work differently when exposed to salt solutions of individual ions as compared with the actual electroplating wastewater. The phenomenon can be caused by the complex chemical composition of the electroplating wastewater, which are characterized by fluctuating states of equilibrium that change over time. In the case of electroplating wastewater, the best flux values were obtained for membranes A and B, slightly lower for composite membrane C, and the lowest volumetric permeate flux values were recorded for unmodified membrane (membrane "0").

3.3. Separation properties of membranes

Investigating the transport properties (Fig. 3) of the obtained membranes, the rejection coefficient of both individual ions and the ions in the electroplating wastewater (Fig. 4) was analyzed in terms of the use of the membranes for heavy metals removal.

Examination of the separation properties (Fig. 4) showed that the Zn^{2+} and Co^{2+} ions were completely removed ($R = 100\%$) on each of the membranes obtained in the experiment, and the abovementioned flux through the membranes is high. Approximate values of rejection coefficient were recorded during the separation of nickel ions, and were: 97.50% (membrane "0"), 96.42% (membrane A), 100% (membrane B) and 98.92% (membrane C), respectively. Not much lower R values for lead ions were determined for pure PAN membrane (96.42%), membrane A (85.17%), membrane B (97.17%) and membrane C (96.92%). However, low rejection coefficient for sodium ions (≈ 20%) indicates that we have obtained an UF membrane.

The high values of the rejection coefficient (Fig. 4) and good transport properties (Fig. 3) confirm that the membranes obtained in the experiment can be successfully used to remove heavy metals such as zinc, nickel, cobalt and lead.

Industrial effluents, including electroplating wastewater, are much more difficult to study. The positive results obtained during the abovementioned studies on the removal of heavy metals from aqueous solutions (Fig. 4) have led us to the use of both pure PAN membranes and MWCNT/PAN composite membranes for the treatment of electroplating wastewater with the composition shown in Table 2.

As a result of the UF (Fig. 5) on the prepared membranes, it was observed that Ni^{2+} ions are removed from the wastewater in 100%. The result obtained was achieved for each of the tested membranes, which coincides with the results obtained in Fig. 4 and may be associated with a low metal concentration (0.03 mg/L) in the wastewater. When analyzing successive results, it can be seen that the removal of the remaining ions in the wastewater (Fig. 5) is not similar to the results obtained for individual ions (Fig. 4). A high degree of removal was obtained for Pb^{2+} ions if MWCNT/PAN composite membranes were used. The rejection coefficient for the successive membranes was: 96.17% (membrane A), 100% (membrane B) and 93.33% (membrane C). Lead(II) ions were the least removed on the membrane "0," because the R-factor was 65.22%. The obtained results are satisfactory due to the fact that the concentration of lead ions in the electroplating wastewater was the highest (2.07 mg/L). The remaining metal ions are also removed in large quantities. The rejection coefficient for zinc(II) ions, with the initial concentration of 0.61 mg/L, was 72 ÷ 79%. Nickel(II) ions, on the other hand, with the initial concentration of 0.05 mg/L, were removed in 70 ÷ 83%. The results obtained (Fig. 5) may indicate the occurrence of competitive reactions leading to preferential removal of metals from the electroplating wastewater.

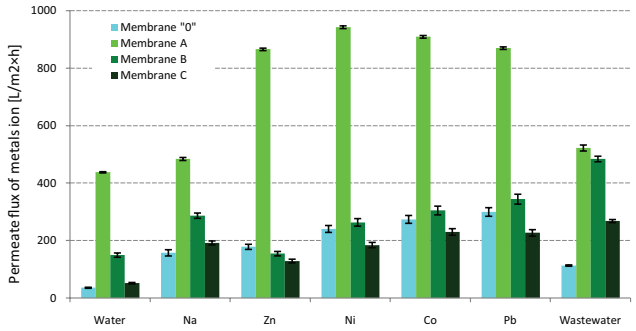

Fig. 3. Volumetric permeate flux values for membranes working in the ionic environment of selected metals and electroplating wastewater (transmembrane pressure of 0.2 MPa).

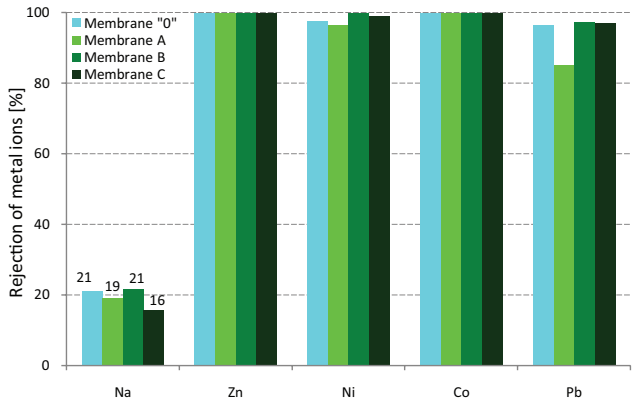

Fig. 4. Rejection coefficient for individual metal ions on subsequent membranes.

3.4. Characterization techniques

3.4.1. SEM analysis

Scanning electron microscopy (SEM) enabled the observation of surface morphology of the skin layer and cross-sections of pure PAN membrane (membrane "0") and MWCNT/PAN composite membranes.

In Fig. 6-1, we can observe that all obtained membranes have an asymmetric structure. Membrane "0" has a thickness of approximately 120 μm and is composed of a pronounced skin layer with a thickness of 10 μm as well as a support layer. The support layer is made of large chambers, whose walls have a porous structure. The cross-sectional morphology

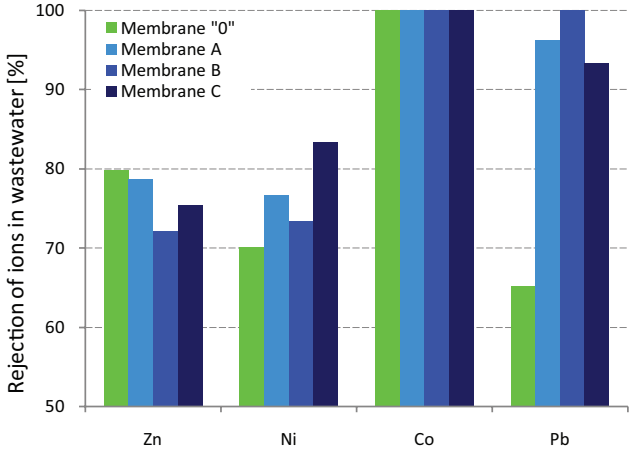

Fig. 5. Rejection coefficient of metal ions in electroplating wastewater on subsequent membranes.

confirms the physicochemical properties discussed earlier (Table 3) and the resulting transport properties (Fig. 2(a)). For MWCNT/PAN composite membranes, in the cross-section images (Fig. 6-1), it is observed that the addition of a modifier to PAN results in the increase of the membranes thickness twice. The thickness of membrane A is 230 μm and the skin is approximately 1.3% of the entire membrane, that is, about 3 ÷ 4 μm. In the image of the cross-section, it can be seen that the support layer is composed of a large number of chambers surrounded by thin layers of a polymer with a very fine porous structure. This construction of the membrane A allows to obtain very good transport properties (Fig. 2(a)). The thickness of membranes B and C is similar to that of membrane A and is approximately 210 ÷ 220 μm. In the cross-sectional images (Fig. 6-1) of the MWCNT/PAN composite membranes it can be observed that as the amount of nanotubes in the polymer matrix decreases, the amount of chambers in the skin layer is reduced. In addition, the layers of polymer that surrounds the chambers form the porous structures visible in the images (Fig. 6-1).

When analyzing the SEM images of the skin layer (Fig. 6-2), a flat surface is observed for membrane "0," which begins to fold slightly (membrane A), and, with the further amount of modifier (MWCNT), results in wrinkles observed on membrane C. Moreover, the images of composite membranes show few small lumps. The structure of the support layer (Fig. 6-3), on the other hand, is three-dimensional, richer in the hollows, openings and pores that increase in number with the amount of MWCNT addition in the PAN matrix.

3.4.2. XRD analysis

Fig. 7 shows wide-angle X-ray scattering (WAXS) diffraction curves of composite MWCNT/PAN membranes studied.

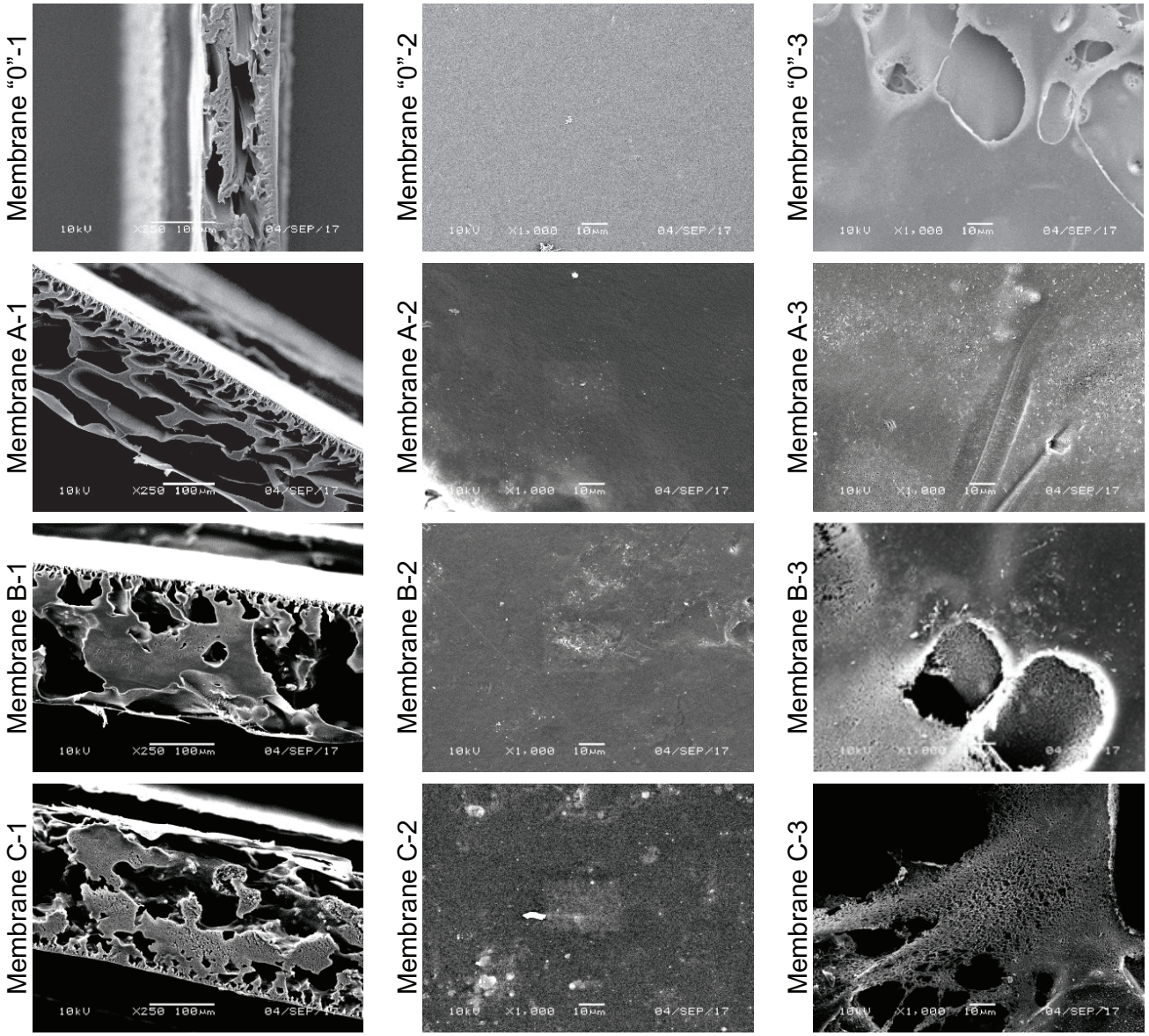

Fig. 6. Images (SEM) of pure PAN and MWCNT/PAN composite membranes: (1) cross-section; (2) skin layer and (3) bottom layer.

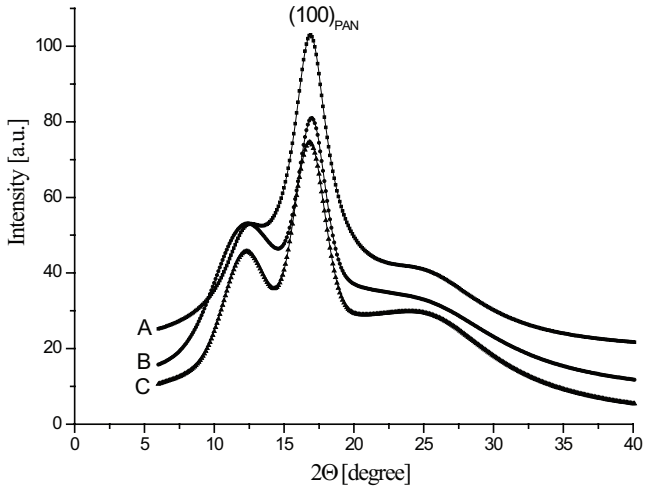

Fig. 7. WAXS patterns of MWCNT/PAN membranes.

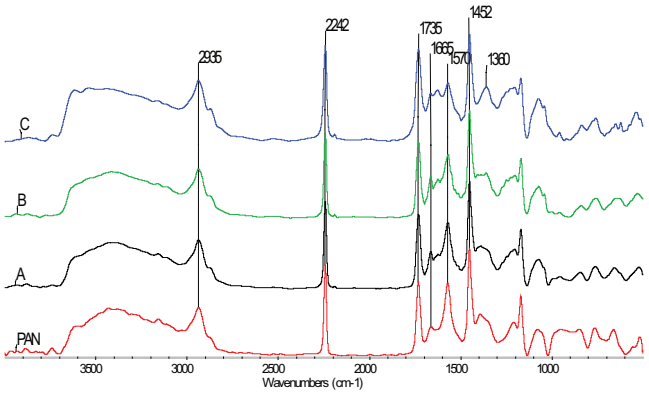

Fig. 8. FTIR spectra of MWCNT/PAN composite membranes (membranes A–C) and pure PAN membrane (membrane "0").

The diffraction curves are dominated by a sharp, intense peaks at 2θ = 12.3° and 16.7°. The peak at 2θ = 16.7° is corresponding to the (100) diffraction of the hexagonal lattice of PAN. The peak at 12.3° is not associated with the structure of the PAN, but may be derived from the nanotubes that form an ordered structure.

To quantitatively examine the crystallinity of the membranes, their crystallinity index was evaluated from WAXS measurements. For this purpose each WAXS curve was deconvoluted into crystalline and amorphous scattering components using the profile fitting program WaxsFit [27]. Each peak was modelled using a Gaussian–Cauchy peak shape. The crystallinity index was calculated as a ratio of the area under crystalline peaks to the total area of the scattering curve. It was found that the crystallinity of the membranes decreased as the nanotube content increased. This is because MWCNT reduced mobility of PAN chains, thereby hindering the crystal formation. Calculated crystallinity index of membrane A was found to be 0.45, whereas for membranes B and C the values of this parameter equal to 0.27 and 0.23, respectively.

3.4.3. FTIR analysis

The molecular structure of the skin surface was investigated using photoacoustic detector in Fourier transform infrared (FTIR) spectroscopy (Fig. 8). Spectra of individual membranes contain characteristic oscillator absorption bands occurring in the PAN: at wave number 2,935 cm^{-1} these are C–H oscillators stretching vibrations; the maximum at the 2,242 cm^{-1} are the stretching vibration of the C≡N oscillator; while the bands at wave numbers 1,452 and 1,360 cm^{-1} are deformation vibrations in the CH_2 and C–H groups. Spectral bands at wavelengths of approximately 1,735 cm^{-1} are characteristic for the stretching vibrations of the C=O oscillator in ester groups and can be derived from the raw PAN (copolymer containing about 6% of methyl acrylate). Analyzing the individual bands in the PAN and MWCNT/PAN composite spectra, it can be seen that the introduction of successive batches of nanotubes into the PAN matrix causes a gradual decrease in C≡N oscillator band intensity, in the direction from membrane A, through B, to C. Similarly, with the increasing amount of MWCNT addition in subsequent membranes, the intensity of the bands at wavelengths 1,665 and 1,570 cm^{-1}, characteristic of the S=O oscillator in acids and sulphonic salts (0.3 wt% of the PAN copolymer is methallyl sulphonate). This may indicate strong interactions between MWCNT and the polymer matrix.

3.4.4. Thermal analysis

3.4.4.1. DSC At the beginning of the calorimetric studies of the MWCNT/PAN membranes, it was necessary to determine the proper heating rate applied throughout the measurement series.

For a speed of 10°/min, most commonly used in classical DSC measurements, the curves (Fig. 10) clearly show that the evaporation of water overlaps with the effect which, based on the analysis of literature [28,29], is to be associated with glass transition within the unorganized PAN phase. In addition, at much higher temperatures we can observe the beginning of the PAN thermal degradation process, well-known from Lee et al. [30], consisting in the first stage of cyclization of the polymer chains. Based on the previous experience of the authors in the studies of modified PAN membranes (Fig. 9), it can be concluded that, with significant changes in the dynamics of the temperature variation as a function of the measurement time (up to 60°/min), pronounced peaks of paracrystalline PAN phase and non-isothermic crystallization occurring during cooling of the alloy are also reflected in the curve.

However, in the case of MWCNT/PAN membranes discussed in this paper, the analysis of the DSC curves does not show the abovementioned effects, despite the fact that the results of the WAXS diffraction studies presented previously clearly show the existence of the hexagonal lattice of PAN, as evidenced by a clear peak at 2θ = 16.7°. Therefore, it was decided that the DSC curves would be recorded at a standard heating rate of 10°/min (Fig. 10).

Analyzing the curves shown in Fig. 10 in the order of increasing temperature, as indicated earlier, in a wide range from 20°C to approximately 120°C, the occurrence of the endothermic peak of the release of water contained in the membrane structure combined with the disturbance of the calorimetric

signal line corresponding to the glass transition, should be noted. No separation of the above transformations and their relatively low intensity practically prevents deeper interpretation. The exception is the minimum temperature of the water evaporation endotherm $T_{w,ev}$, whose changes are strictly compatible with the previously reported results for pore size and membrane transport properties studies. This temperature is definitely the highest for membrane "0" (76.9°C), then it abruptly decreases to 68.0°C and monotonically increases for individual composite membranes with an increase in MWCNT modifier content (Table 4).

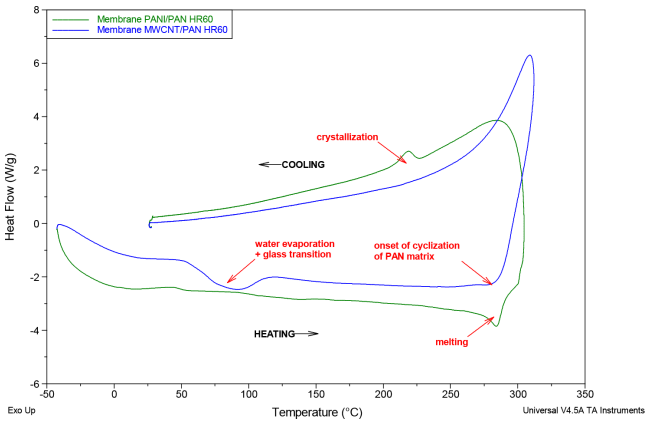

Fig. 9. DSC curves registered in relatively heating and cooling rates of 60°C/min for composite membranes obtained from PAN modified with: polyaniline (green) and MWCNT (blue), respectively.

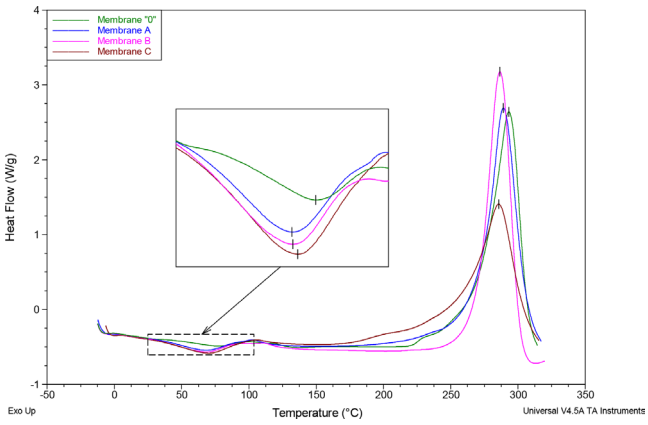

Fig. 10. DSC curves for investigated membranes obtained from: unmodified PAN (green), and PAN modified with MWCNT: 0.83% (blue), 4.2% (pink) and 8.3% (maroon), respectively. Analysis of temperature ranges of water evaporation and cyclization of PAN.

For all tested membranes, at temperatures just below 300°C, the curves show a very strong exothermic peak, which is the dominant element of the thermogram. The discussed thermal effect reflects the PAN cyclization reaction that occurs during heating. According to Lee et al. [30], the PAN homopolymer is cyclized as a result of free-radical reaction at a temperature of 306.2°C. In our case, PAN used to prepare membranes is a copolymer, and its cyclization temperature is 293.2°C (specific enthalpy of cyclization of 578.0 J/g). Whereas the cyclization temperatures for the other membranes, modified using MWCNT, are slightly lower: 289.2°C (membrane A), 286.6°C (membrane B) and 285.8°C (membrane C). This behaviour of the samples of the composite membranes is confirmed by the results described by Poochai and Pongprayoon [31], where the values of the specific enthalpy of the transformation show no specific tendency of change.

3.4.2. TGA As part of this study, TGA investigation of the membranes was mainly used to show the influence of the MWCNT modifier used on the thermal decomposition of the PAN matrix. The thermal stability of PAN composite with the addition of CNTs has previously been investigated inter alia by Song and Xu [18] and Palade et al. [20]. Fig. 11 summarizes the weight loss curves of thermogravimetric (TG) and derivative thermogravimetric (dTG) differential curves registered for all the membranes discussed in the paper.

The analysis of the curves shows the thermal stability of the composite membranes up to approximately 250°C. Membrane "0," on the other hand, shows much higher thermal stability – up to 300°C it loses only 1.7% of its mass. This confirms the results of the DSC studies, also reflected in the previously mentioned work [31]. The predominant effect on the TG curves for all tested membranes is the fundamental loss in weight associated with the thermal dissociation of PAN. This process takes place in many stages (with the highest number of stages in the case of membrane C), wherein the stages are not completely separated temperature-wise (the dTG signal between them is not 0). For the first decomposition stage, the highest weight loss rate for membrane "0," free of the MWCNT modifier, occurs at 342.1°C, and for composite membranes decreases by several dozen degrees with decreasing content of nanotubes. At this stage, membrane "0"

Table 4
Values of temperatures and enthalpies of: water evaporation and PAN cyclization, respectively, evaluated on the basis of DSC curves (Fig. 9) for investigated MWCNT/PAN membranes

Sample	Temperature of water evaporation	Temperature of PAN cyclization	Enthalpy of PAN cyclization
	$T_{w,ev}$ (°C)	T_c (°C)	DH_c (J/g)
Membrane "0"	76.9	293.2	578.0
Membrane A	68.0	289.2	529.8
Membrane B	68.4	286.6	557.8
Membrane C	70.2	285.8	454.9

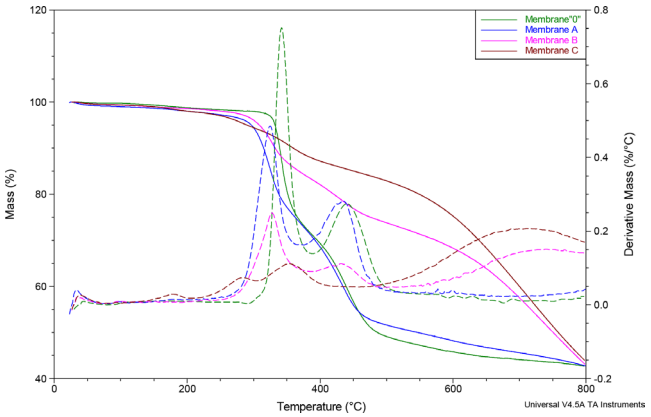

Fig. 11. TG and dTG curves for MWCNT/PAN composite membranes.

is characterized by the highest loss of weight (28.3%), while membrane C by the lowest (only 4.1%). For the latter, the thermal dissociation of the PAN matrix is slightly different and its first symptoms are already observed slightly below 180°C. In the second stage of PAN thermal dissociation, the highest weight loss rate is observed in a much wider range of temperatures: from 354.3°C (membrane C) to 440.6°C (membrane "0"). It can be assumed that the discussed decomposition stage for membranes containing less than 1% of nanotubes ends at about 510°C, and the sample residues – carbonates represent about half of their initial mass (48.6% for membrane "0" and 51.2% of membrane A). At higher MWCNT contents, the sample residues in the discussed temperature range are significantly higher (up to 83.3% in case of membrane C). The formation of proper carbonates is associated with an additional decomposition stage and is shifted towards temperatures substantially above 800°C (range beyond Fig. 11).

4. Conclusions

The aim of the research was to obtain composite membranes from PAN with MWCNT addition and to inspect their applicability for removing heavy metals. The introduction of the MWCNT additive into the PAN matrix slowed down the membrane coagulation process, which resulted in an increase in their mass per unit area, thickness, apparent density and porosity, and improved the transport properties. Of all the composite membranes MWCNT/PAN obtained, the membrane A was characterized by the best properties. The pure water flux through membrane A was 10-fold higher than in the unmodified membrane (membrane "0"). Therefore, the PAN modification with a small amount of MWCNT (0.83% w/w) caused that "fast" high flux membranes were obtained.

Satisfactory results of transport research prompted to analyze the separation properties of composite membranes MWCNT/PAN. The test results indicated that UF membranes were obtained because they were characterized by a low rate of sodium ions retention ($R \approx 20\%$) and a high removal rate of zinc, nickel, cobalt and lead ions (~100%). At the same time, a phenomenon not described in the literature was observed, consisting in a two-fold increase in the volumetric value of the permeate stream during the permeation of inorganic salt solutions.

Performing structural tests allowed to explain phenomena observed during physicochemical properties tests. When analyzing the SEM photomicrographs, it can be seen that the best structural structure is characterized by membrane A. The use of WAXS and DSC techniques allowed to observe the drop in the crystallinity of PAN in composite membranes with the increase in the amount of MWCNT in the composite. The obtained results confirm the good dispersion of MWCNT in the PAN matrix. FTIR spectroscopy allowed to observe the bonds between components of the MWCNT/PAN composite.

References

[1] X. Zhao, G. Zhang, Q. Jia, C. Zhao, W. Zhou, W. Li, Adsorption of Cu(II), Pb(II), Co(II), Ni(II), and Cd(II) from aqueous solution by poly(aryl ether ketone) containing pendant carboxyl groups (PEK-L): equilibrium, kinetics, and thermodynamics, Chem. Eng. J., 171 (2011) 152–158.
[2] H.A. Aziz, M.N. Adlan, K.S. Ariffin, Heavy metals (Cd, Pb, Zn, Ni, Cu and Cr(III)) removal from water in Malaysia: post treatment by high quality limestone, Bioresour. Technol., 99 (2008) 1578–1583.
[3] Q. Chen, Z. Luo, C. Hills, G. Xue, M. Tyrer, Precipitation of heavy metals from wastewater using simulated flue gas: sequent additions of fly ash, lime and carbon dioxide, Water Res., 43 (2009) 2605–2614.
[4] M. Li, Z. Zhang, R. Li, J.J. Wang, A. Ali, Removal of Pb(II) and Cd(II) ions from aqueous solution by thiosemicarbazide modified chitosan, Int. J. Biol. Macromol., 86 (2016) 876–884.
[5] F. Ferniza-García, A. Amaya-Chávez, G. Roa-Morales, C.E. Barrera-Díaz, Removal of Pb, Cu, Cd, and Zn present in aqueous solution using coupled electrocoagulation-phytoremediation treatment, Int. J. Electrochem., 2017 (2017) 1–11.
[6] V.K. Gupta, O. Moradi, I. Tyagi, S. Agarwal, H. Sadegh, R. Shahryari-Ghoshekandi, A.S.H. Makhlouf, M. Goodarzi, A. Garshasbi, Study on the removal of heavy metal ions from industry waste by carbon nanotubes: effect of the surface modification: a review, Crit. Rev. Environ. Sci. Technol., 46 (2016) 93–118.
[7] R. Saito, G. Dresselhaus, M.S. Dresselhaus, Physical Properties of Carbon Nanotubes, 1st ed., Imperial College Press, London, 1998.
[8] H. Mahmoodian, O. Moradi, B. Shariatzadeha, T.A. Salehf, I. Tyagi, A. Maity, M. Asif, V.K. Gupta, Enhanced removal of methyl orange from aqueous solutions by poly HEMA-chitosan-MWCNT nano-composite, J. Mol. Liq., 202 (2015) 189–198.
[9] S. Majeed, D. Fierro, K. Buhr, J. Wind, B. Du, A. Boschetti-de-Fierro, V. Abetz, Multi-walled carbon nanotubes (MWCNTs) mixed polyacrylonitrile (PAN) ultrafiltration membranes, J. Membr. Sci., 403–404 (2012) 101–109.
[10] M.R. Mahdavi, M. Delnavaz, V. Vatanpour, J. Farahbakhsh, Effect of blending polypyrrole coated multiwalled carbon nanotube on desalination performance and antifouling property of thin film nanocomposite nanofiltration membranes, Sep. Purif. Technol., 184 (2017) 119–127.
[11] S. Kumar, A. Sharma, B. Tripathi, S. Srivastava, S. Agrawal, M. Singh, K. Awasthi, Y.K. Vijay, Enhancement of hydrogen gas permeability in electrically aligned MWCNT-PMMA composite membranes, Micron, 41 (2010) 909–914.
[12] G. Kaminska, J. Bohdziewicz, J.I. Calvo, P. Pradanos, L. Palacio, A. Hernandez, Fabrication and characterization of polyethersulfone nanocomposite membranes for the removal of endocrine disrupting micropollutants from wastewater. Mechanisms and performance, J. Membr. Sci., 493 (2015) 66–79.
[13] N. El Badawi, A.R. Ramadan, A.M.K. Esawi, M. El-Morsi, Novel carbon nanotube-cellulose acetate nanocomposite membranes for water filtration applications, Desalination, 344 (2014) 79–85.
[14] L.D. Tijing, Y.C. Woo, W.G. Shim, T. He, J.S. Choi, S.H. Kim, H.K. Shon, Superhydrophobic nanofiber membrane containing carbon nanotubes for high-performance direct contact membrane distillation, J. Membr. Sci., 502 (2016) 158–170.

[15] M.H. Davood Abadi Farahani, D. Hua, T.S. Chung, Cross-linked mixed matrix membranes consisting of carboxyl-functionalized multi-walled carbon nanotubes and P84 polyimide for organic solvent nanofiltration (OSN), Sep. Purif. Technol., 186 (2017) 243–254.
[16] S. Roy, M. Bhadra, S. Mitra, Enhanced desalination via functionalized carbon nanotube immobilized membrane in direct contact membrane distillation, Sep. Purif. Technol., 136 (2014) 58–65.
[17] H. You, X. Li, Y. Yang, B. Wang, Z. Li, X. Wang, M. Zhu, B.S. Hsiao, High flux low pressure thin film nanocomposite ultrafiltration membranes based on nanofibrous substrates, Sep. Purif. Technol., 108 (2013) 143–151.
[18] Y. Song, L. Xu, Permeability, thermal and wetting properties of aligned composite nanofiber membranes containing carbon nanotubes, Int. J. Hydrogen Energy, 42 (2017) 19961–19966.
[19] Z. Xu, X. Li, K. Teng, B. Zhou, M. Ma, M. Shan, K. Jiao, X. Qian, J. Fan, High flux and rejection of hierarchical composite membranes based on carbon nanotube network and ultrathin electrospun nanofibrous layer for dye removal, J. Membr. Sci., 535 (2017) 94–102.
[20] S. Palade, A. Pantazi, S. Vulpe, C. Berbecaru, V. Ţucureanu, O. Oprea, R.F. Negrea, D. Dragoman, Tunable dielectric properties in polyacrylonitrile/multiwall carbon nanotube composites, Polym. Compos., 38 (2015) 1741–1748.
[21] Z. Dastbaz, M. Pakizeh, M. Namvar-Mahboub, The effect of functionalized MWCNT and SDS on the characteristic and performance of PAN ultrafiltration membrane, Desal. Wat. Treat., 3994 (2016) 1–11.
[22] G. Wypych, Handbook of Polymers, 2nd ed., ChemTec Publishing, Ontario, Canada, 2016, pp. 271–275.
[23] S. Zinadini, A.A. Zinatizadeh, M. Rahimi, V. Vatanpour, H. Zangeneh, Preparation of a novel antifouling mixed matrix PES membrane by embedding graphene oxide nanoplates, J. Membr. Sci., 453 (2014) 292–301.
[24] B. Fryczkowska, L. Przywara, T. Turek, Application of PAN/PANI composite membranes in purification of industrial wastewater generated during processing of metals, Ecol. Eng., 18 (2017) 21–29.
[25] L.P. Beata Fryczkowska, The effect of the type of admixture on the properties of polyacrylonitrile membranes modified with nanotubes, graphene oxide and graphene, J. Ecol. Eng., 18 (2017) 72–81.
[26] Y. Feng, G. Han, L. Zhang, S.-B. Chen, T.-S. Chung, M. Weber, C. Staudt, C. Maletzko, Rheology and phase inversion behavior of polyphenylenesulfone (PPSU) and sulfonated PPSU for membrane formation, Polymer, 99 (2016) 72–82.
[27] M. Rabiej, Application of the particle swarm optimization method for the analysis of wide-angle X-ray diffraction curves of semicrystalline polymers, J. Appl. Crystallogr., 50 (2017) 221–230.
[28] Z. Bashir, The hexagonal mesophase in atactic polyacrylonitrile: a new interpretation of the phase transitions in the polymer, J. Macromol. Sci., Phys., 40 (2001) 41–67.
[29] Z. Bashir, S.P. Church, D. Waldron, Interaction of water and hydrated crystallization in water-plasticized polyacrylonitrile films, Polymer, 35 (1994) 967–976.
[30] S. Lee, Y.-J. Kim, D.-H. Kim, B.-C. Ku, H.-I. Joh, Synthesis and properties of thermally reduced graphene oxide/polyacrylonitrile composites, J. Phys. Chem. Solids, 73 (2012) 741–743.
[31] C. Poochai, T. Pongprayoon, Enhancing dispersion of carbon nanotube in polyacrylonitrile matrix using admicellar polymerization, Colloids Surf., A, 456 (2014) 67–74.